

Data-Efficient Brushstroke Generation with Diffusion Models for Oil Painting

DANTONG QIN, Delft University of Technology, Netherlands
 ALESSANDRO BOZZON, Delft University of Technology, Netherlands
 XIAN YANG, The University of Manchester, UK
 XUN ZHANG, Delft University of Technology, Netherlands
 YIKE GUO, The Hong Kong University of Science and Technology, HKSAR
 PAN WANG*, Delft University of Technology, Netherlands

Many creative multimedia systems are built upon visual primitives such as strokes or textures, which are difficult to collect at scale and fundamentally different from natural image data. This data scarcity makes it challenging for modern generative models to learn expressive and controllable primitives, limiting their use in process-aware content creation. In this work, we study the problem of learning human-like brushstroke generation from a small set of hand-drawn samples ($n = 470$) and propose StrokeDiff, a diffusion-based framework with Smooth Regularization (SmR). SmR injects stochastic visual priors during training, providing a simple mechanism to stabilize diffusion models under sparse supervision without altering the inference process. We further show how the learned primitives can be made controllable through a Bézier-based conditioning module and integrated into a complete stroke-based painting pipeline, including prediction, generation, ordering, and compositing. This demonstrates how data-efficient primitive modeling can support expressive and structured multimedia content creation. Experiments indicate that the proposed approach produces diverse and structurally coherent brushstrokes and enables paintings with richer texture and layering, validated by both automatic metrics and human evaluation.

CCS Concepts: • **Applied computing** → **Fine arts**; • **Computing methodologies** → **Computer vision**.

Additional Key Words and Phrases: Brushstroke Synthesis, Stroke-based Rendering, Diffusion Models, Artist Painting, Few-shot

ACM Reference Format:

Dantong Qin, Alessandro Bozzon, Xian Yang, Xun Zhang, Yike Guo, and Pan Wang. 2018. Data-Efficient Brushstroke Generation with Diffusion Models for Oil Painting. *Proc. ACM Meas. Anal. Comput. Syst.* 37, 4, Article 111 (August 2018), 23 pages. <https://doi.org/XXXXXXXX.XXXXXXX>

1 Introduction

Painting is a layered, iterative process in which artists build visual scenes through successive brushstrokes, each carrying spatial, textural, and stylistic intent [3, 28, 55]. In creative multimedia systems, stroke-based rendering (SBR) is a representative paradigm that seeks to emulate this process by synthesizing images as sequences of

*Corresponding author to this work.

Authors' Contact Information: Dantong Qin, D.Q.Dantong@tudelft.nl, Delft University of Technology, Delft, Netherlands; Alessandro Bozzon, A.Bozzon@tudelft.nl, Delft University of Technology, Delft, Netherlands; Xian Yang, xian.yang@manchester.ac.uk, The University of Manchester, Manchester, UK; Xun Zhang, x.zhang-16@tudelft.nl, Delft University of Technology, Delft, Netherlands; Yike Guo, yikeguo@ust.hk, The Hong Kong University of Science and Technology, Kowloon, HKSAR; Pan Wang, P.Wang-2@tudelft.nl, Delft University of Technology, Delft, Netherlands.

Permission to make digital or hard copies of all or part of this work for personal or classroom use is granted without fee provided that copies are not made or distributed for profit or commercial advantage and that copies bear this notice and the full citation on the first page. Copyrights for components of this work owned by others than the author(s) must be honored. Abstracting with credit is permitted. To copy otherwise, or republish, to post on servers or to redistribute to lists, requires prior specific permission and/or a fee. Request permissions from permissions@acm.org.

© 2018 Copyright held by the owner/author(s). Publication rights licensed to ACM.

ACM 2476-1249/2018/8-ART111

<https://doi.org/XXXXXXXX.XXXXXXX>

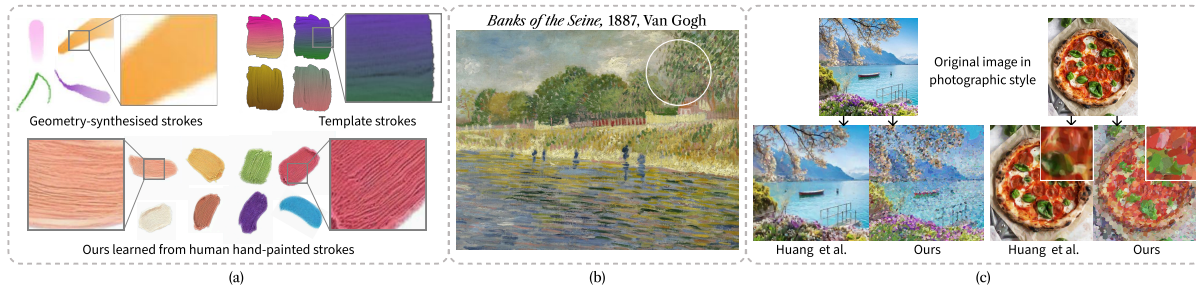


Fig. 1. Comparison of stroke quality and painting outputs. (a) Prior SBR methods use geometric or template strokes with limited expressive capacity. Our strokes, learned from human-painted data, yield richer structure and texture. (b) Target oil painting style, showing abstraction beyond realism. (c) Compared to Huang et al. [22], Our method introduces a stronger artistic domain shift.

discrete brushstrokes. Unlike photorealistic synthesis, SBR does not aim to reproduce pixels but to convey semantic content through painterly representation. Recent methods have made progress in generating content-aligned renderings, yet most rely on predefined stroke templates [19, 33, 42, 48, 50] or geometry-synthesized primitives [22, 36, 45, 53]. While these approaches offer efficiency and structural consistency, they often struggle to capture the diversity, irregularity, and texture of human brushstrokes, which are essential for stylistic abstraction. As a result, the expressive space of human-like strokes remains underexplored in data-driven painting pipelines (see Fig. 1 for comparison).

To address this gap, we investigate the problem of generating human-like brushstrokes using diffusion models (DMs). Compared to natural image domains, where large-scale datasets are widely available, real brushstroke data remain scarce and underexplored in existing literature. Compared to earlier approaches such as GAN-based stroke synthesis [25, 36, 53], DMs excel when trained on abundant data, but their ability to generalize to design-time primitives is less understood, and direct fine-tuning of pretrained models on a few hundred samples tends to result in structural degradation. This highlights the challenge of stabilizing diffusion training under limited data while maintaining the abstraction and stylistic qualities of artistic strokes.

Previous efforts to address low-resource diffusion have either modified the diffusion path (e.g., noise scheduling [5, 9, 13, 30, 32, 58]), classifier (or classifier-free) guidance [6, 7, 12]) or inject external conditions such as prompts [8, 37] or exemplars [16, 26, 40, 56]. While effective in some domains, these strategies often require large-scale tuning or introduce test-time dependencies, which limits their scalability. In this work, we propose **StrokeDiff**, a diffusion-based framework designed for learning expressive visual primitives under extremely limited data. At its core is **Smooth Regularization (SmR)**, a training-time strategy that injects *stochastic visual priors* into the forward diffusion process to compensate for the lack of structural supervision. By injecting weak but diverse visual cues during training, SmR encourages the model to preserve global structure and semantic coherence in low-signal regimes. Importantly, SmR operates purely at training time and does not modify the inference procedure or require additional conditions. This makes it a lightweight and general regularizer for stabilizing diffusion models under sparse data, without introducing test-time dependencies or computational overhead.

Beyond individual strokes, to demonstrate that the learned primitives can support structured content creation, we further introduce a Bézier-parametrized conditioning module that enables controllable stroke synthesis and facilitates integration into painting pipelines. This design provides explicit control over stroke attributes such as shape and placement, and supports their arrangement into complete images. To further improve composition, we add a ranking loss that regularizes stroke order, mitigating overlap artifacts and enhancing stylistic layering.

Our experiments indicate that StrokeDiff generates high-fidelity and diverse strokes from 470 hand-drawn samples, generalizes better than noise scheduling and LoRA-based adaptation under sparse data. At the level of complete paintings, it produces more coherent and stylistically expressive results, which we evaluate using both semantic metrics such as CLIP alignment and human preference studies that assess style, texture, and overall aesthetic quality. Our main contributions are:

- Smooth Regularization (SmR): a training-time regularization strategy based on stochastic visual prior injection, which stabilizes diffusion training under sparse data without modifying the inference procedure.
- Controllable stroke synthesis and pipeline integration: we design a Bézier-parametrized conditioning module for controllable stroke generation, and connect it with a complete painting pipeline, leading to brushstroke renderings that better capture the layering and textural qualities of oil painting.
- Evaluation: we conduct multi-dimensional evaluation at both the stroke and painting levels, using CRD, FID, LPIPS, and human studies to compare template-, vector-, GAN-, and diffusion-based approaches.

2 Related work

2.1 Strokes in Stroke-Based Rendering

While generative models have also made progress in image stylization [21, 38, 54], stroke-based rendering constructs images through sequential brushstrokes, emulating the layered approach of human artists [22, 23, 34, 44, 45]. Existing methods can be broadly categorized into template-based, neural stroke generation, and vector graphics-based approaches. Template-based approaches [18, 19, 33, 42, 49, 50] transform a limited set of stroke templates through parameter adjustments (e.g., color, length, and angle). While they preserve the appearance of painting textures, their reliance on fixed templates often leads to repetitive stroke patterns. Neural stroke generation methods [36, 53, 61] aim to increase stroke diversity by synthesizing strokes from noise. However, many of these models are trained on synthetic datasets (e.g., MyPaint¹ or FluidPaint²), leading to overly smooth and geometric outputs. Although Bidgoli et al. [1] trained a VAE on real brushstrokes, their method was not integrated into a complete painting pipeline. Another line of work employs vector graphics-based approaches [4, 17, 22, 29] to fit brushstrokes as parametric curves, such as Bézier splines. While these methods achieve strong structural fidelity, they often sacrifice the spontaneity and organic variation found in freehand painting. Despite advances in SBR, achieving diverse, realistic, and expressive brushstrokes remains a core challenge.

2.2 Low-data diffusion methods

Recent work has adapted diffusion models to low-data regimes by incorporating external priors or prompts to guide generation, including exemplar-based personalization methods such as DreamBooth [40] and Custom Diffusion [26], or inversion-based approach [35], and attention manipulation techniques [10, 46]. While effective for high-fidelity or controllable generation, these methods typically rely on test-time inputs or prompt engineering, and are often constrained to instance-specific synthesis. Another line of research focuses on improving sample diversity under constrained training by modifying the diffusion path through noise scheduling [5, 9, 13, 30], or posterior guidance [12], or multi-stage refinement frameworks such as DoD [59], which incorporate visual priors from earlier stages to enhance semantic structure and fidelity. Our method introduces a training-time modification to the diffusion path yet maintains no test-time conditions.

3 Method

Our goal is to train a diffusion model on a small set of hand-drawn brushstrokes, enabling it to generate strokes that are human-like in both texture and structure. The proposed framework, *StrokeDiff*, augments standard latent

¹<https://github.com/mypaint/mypaint>

²<https://david.li/paint/>

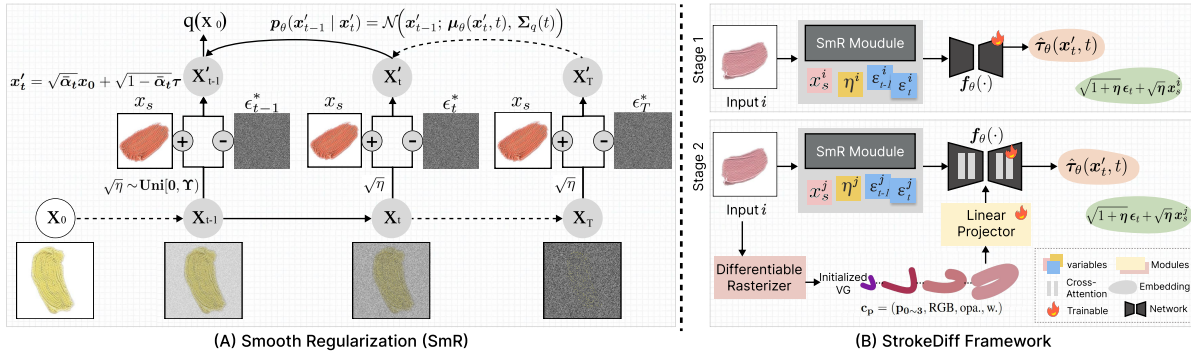


Fig. 2. Overview of our method. (A) Smooth Regularization injects priors during training to mitigate mode collapse under limited data. At each timestep, a brushstroke x_s is sampled from the dataset and injected into the forward process alongside a newly sampled noise term $\epsilon^* \sim \mathcal{N}(0, I)$; both terms are scaled by a factor $\eta \sim \text{Uni}[0, \Upsilon]$. (B) The StrokeDiff framework is trained in two stages. In Stage 1, the model learns to generate strokes with SmR but without conditional inputs. In Stage 2, we incorporate parameter conditioning via a raster-to-vector module that predicts vectorized stroke parameters (e.g., control points, opacity, RGB, width). These parameters are then used to control the generation of specific brushstroke attributes.

diffusion with visual prior injection and stroke-level controllability (see Fig. 2 for an overview). We begin by training the model without inference-time conditioning, and introduce *Smooth Regularization (SmR)* to inject weak visual priors during training, mitigating the mode collapse observed when fine-tuning a latent diffusion model (LDM) by modifying the diffusion process. SmR is applied only during training and deactivated at inference, which allows standard noise sampling without additional preparation. To make the outputs compatible with downstream tasks, we further parameterize brushstrokes and support controllable generation based on stroke attributes. These components together allow StrokeDiff to serve both as a stand-alone stroke generator and as the foundation of a broader painting pipeline, which we detail later in this section.

3.1 Preliminaries

Diffusion models generate samples by iteratively denoising an initial Gaussian noise input. In the forward process, a clean image x_0 is gradually corrupted by adding Gaussian noise in a Markov chain. One way to express this is:

$$q(x_t | x_{t-1}) = \mathcal{N}(x_t; \sqrt{\alpha_t} x_{t-1}, (1 - \alpha_t)I), \quad (1)$$

where α_t controls how much information from x_{t-1} is retained. By applying this step repeatedly from $t = 1$ to T , we can write a closed-form distribution conditioned on x_0 :

$$q(x_t | x_0) = \mathcal{N}(x_t; \sqrt{\bar{\alpha}_t} x_0, (1 - \bar{\alpha}_t)I), \quad (2)$$

where $\bar{\alpha}_t = \prod_{i=1}^t \alpha_i$.

To invert this process, a neural network $\epsilon_\theta(x_t, t)$ is trained to predict the noise $\epsilon \sim \mathcal{N}(0, I)$ added to x_0 , minimizing

$$\mathcal{L}(\theta) = \mathbb{E}_{x_0, \epsilon, t} [\|\epsilon - \epsilon_\theta(x_t, t)\|^2]. \quad (3)$$

Using these predictions, the reverse transition is:

$$p_\theta(x_{t-1} | x_t) = \mathcal{N}(x_{t-1}; \mu_\theta(x_t, t), \Sigma_q(t)), \quad (4)$$

where $\mu_\theta(x_t, t)$ and $\Sigma_q(t)$ guide the reconstruction of x_0 .



Fig. 3. Stroke generation using Stable Diffusion v1-5 [39] fine-tuned on typical stroke data that lacks sufficient diversity. Due to severe mode collapse early in training, the model produces only texture-like images with minimal variation and no authentic brushstroke resemblance.

3.2 High-fidelity stroke generation with visual guidance

3.2.1 Problem Setting. Our work focuses on learning to generate brushstroke primitives collected from a single artist, comprising 470 scanned strokes. These primitives represent process-oriented visual elements that are rarely observed independently in public datasets, which are fundamentally out-of-distribution for open-domain latent diffusion models, making them unrecoverable via prompt tuning or conditional guidance. The direct fine-tuning of Stable Diffusion 1.5 on this dataset leads to severe mode collapse (see Fig. 3). While the strokes exhibit family-level stylistic coherence, they are semantically sparse and structurally diverse, leading to a low information density problem. As a result, the fine-tuned model fails to infer global structure during the early denoising steps. Given the low-frequency structures could require longer temporal horizons to learn [13], we hypothesize that the weak semantic signal is rapidly overwhelmed by noise under standard diffusion schedules. To address this, we propose a regularization strategy to facilitate structure preservation in low-signal regimes.

3.2.2 Stochastic Visual Prior. We introduce a *visual prior* x_s at each diffusion step. Rather than relying solely on noisy reconstructions of the target stroke, we sample x_s a random brushstroke from the training set, leveraging inter-stroke consistency to provide structure-aware guidance. The modified forward process is defined as:

$$x'_t = \boxed{x_t} + \boxed{\sqrt{1 - \bar{\alpha}_t} \sqrt{\eta} x_s} - \boxed{\sqrt{1 - \bar{\alpha}_t} \sqrt{\eta} \epsilon_t^*}, \quad (5)$$

where η is a scaling factor (sampled from $\text{Uni}[0, \Upsilon]$, $0 < \Upsilon < 1$) that modulates the strength of prior injection. It is sampled once per training instance and shared across timesteps. Notably, $\bullet x'_t$ does not follow from x'_{t-1} , $\bullet x_t$ is interpolated with x_s at each timestep, and $\bullet \epsilon_t^* \sim \mathcal{N}(0, I)$ is a newly sampled noise added to maintain diversity by increasing overall variance. Otherwise, the additional structure would reduce the noise magnitude and potentially bias training. The resulting distribution $q(x'_t | x_0)$ includes both a data term $\sqrt{\bar{\alpha}_t} x_0$ and a visual prior term $\sqrt{1 - \bar{\alpha}_t} \sqrt{\eta} x_s$, as shown below:

$$= \mathcal{N}\left(x'_t; \underbrace{\sqrt{\bar{\alpha}_t} x_0}_{\text{Data Term}} + \underbrace{\sqrt{1 - \bar{\alpha}_t} \sqrt{\eta} x_s}_{\text{Visual Prior}}, \underbrace{(1 + \eta)(1 - \bar{\alpha}_t) \mathbf{I}}_{\text{Variance Term}}\right). \quad (6)$$

The visual prior x_s does not propagate across timesteps. As a result, the injected structure remains temporally local and does not accumulate through the trajectory. This non-propagating nature prevents the model from memorizing fixed structural patterns, in contrast to deterministic scheduling schemes where the noise trajectory is predefined across steps and samples.

We derive a modified posterior distribution that $q(x'_{t-1} | x'_t, x_0)$

$$\propto \mathcal{N}\left(x'_{t-1}; \frac{\sqrt{\bar{\alpha}_t}(1 - \bar{\alpha}_{t-1})(1 + \eta)x'_t + \sqrt{\bar{\alpha}_{t-1}}((1 - \alpha_t - 2\bar{\alpha}_t)\eta + 1 - \alpha_t)x_0 + f(\eta)}{1 - \bar{\alpha}_t + (1 + 2\alpha_t - 3\bar{\alpha}_t)\eta}, \frac{((1 + \alpha_t - 2\bar{\alpha}_t)\eta + 1 - \alpha_t)(1 + \eta)(1 - \bar{\alpha}_{t-1}) \mathbf{I}}{1 - \bar{\alpha}_t + (1 + 2\alpha_t - 3\bar{\alpha}_t)\eta}\right). \quad (7)$$

$f(\eta)$ represents the independent term dependent on η , expressed as:

$$f(\eta) = \sum_{k=1}^3 A_k \sqrt{\eta}^k, \quad (8)$$

with coefficients A_k determined by $\alpha_t, \alpha_{t-1}, \bar{\alpha}_t, \bar{\alpha}_{t-1}$, and x_s .

3.2.3 Smooth Regularization. With this formulation, we define τ as an alternative representation of the noise process:

$$\tau = \sqrt{1 + \eta} \epsilon + \sqrt{\eta} x_s, \quad (9)$$

which encapsulates both learned noise and the injected prior. This allows us to parameterize the true denoising transition mean $\mu_q(x'_t, x_0)$ as follows:

$$\frac{\sqrt{\bar{\alpha}_{t-1}}(1 - \bar{\alpha}_t)x'_t + C_1 x'_t - \sqrt{\bar{\alpha}_{t-1}}\sqrt{1 - \bar{\alpha}_t}(1 - \alpha_t)\tau + C_2 \tau + f(\eta)}{\sqrt{\bar{\alpha}_t}(1 - \bar{\alpha}_t + (1 + 2\alpha_t - 3\bar{\alpha}_t)\eta)}, \quad (10)$$

where C_1 and C_2 are coefficients, with each term multiplied with η . Since τ introduces additional stochasticity, the model must learn **both the underlying noise and the prior's effect**. Thus, we parameterize $\hat{\tau}_\theta(x'_t, t)$ via LDM's neural network, which refines the reconstruction process. Then, the optimization problem simplifies to:

$$\mathbf{L}_\tau(\theta) = \mathbb{E} [\|\tau - \hat{\tau}_\theta(x'_t, t)\|^2]. \quad (11)$$

During inference, setting $\eta = 0$ nullifies the visual prior, reducing to:

$$\mu_q(x'_t, t) = \mu_q(x_t, t) \quad \text{in DDPM}, \quad (12)$$

$$\Sigma_q(t) = \Sigma_q(t) \quad \text{in DDPM}. \quad (13)$$

This design remains compatible with existing diffusion sampling strategies, allowing the model to generate images purely from Gaussian noise without any additional priors. Since this approach “smooths” the noise via a modified training objective, we refer to it as *Smooth Regularization*. In practice, it is straightforward to implement. Moreover, because x_s is randomly sampled, each x_0 can pair with multiple distinct priors, effectively enlarging the training set and further boosting stroke diversity.

3.3 Controllable stroke synthesis for downstream applications

Since our brushstrokes originate from scanned images, they lack an inherent parametric form. To introduce parametric control, we adopt a differentiable rasterizer [29] that initializes a simple parametric primitive and iteratively refines it to match the target stroke. Specifically, we set both the path and segment count to 1, approximating each stroke with a single cubic Bézier curve:

$$c_p = (p_0, p_1, p_2, p_3, R, G, B, \text{opacity}, \text{width}), \quad (14)$$

where each p_i holds the (x, y) coordinates of a control point, resulting in $c_p \in \mathbb{R}^{1 \times 13}$. By mapping strokes to this vector-graphic representation, we avoid manually recording brush trajectories [1], thus making our approach compatible with any rasterized brushstroke data.

We integrate this parametric information into the model by concatenating c_p with a contextual feature c (e.g., color or style embedding) and project the combined vector:

$$z = W [c_p; c], \quad (15)$$

where $[\cdot; \cdot]$ denotes vector concatenation, and W is a learnable projection matrix. We then feed z into the U-Net's cross-attention mechanism, fine-tuning both the projector and cross-attention layers. This setup enables conditional stroke generation that follows Bézier-defined shapes while preserving high-fidelity rasterization.

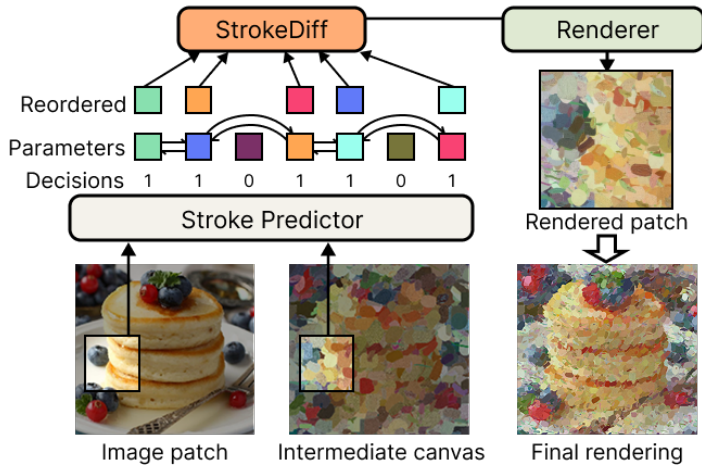


Fig. 4. Illustration of the painting pipeline. Stroke parameters are re-ordered according to the predicted ranking scores scr_r to ensure a coherent rendering sequence.

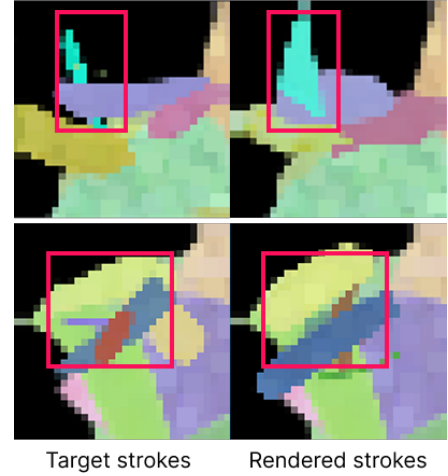


Fig. 5. Strokes that are only optimally matched render an unordered sequence, leading to incorrect overlapping.

3.4 Painting pipeline integration

To render full paintings, we integrate StrokeDiff into a stroke-based rendering pipeline. The process involves (i) predicting stroke parameters (position, shape, size) from a target image, (ii) generating corresponding strokes using our diffusion model, and (iii) compositing them sequentially on a canvas with a renderer, as illustrated in Fig. 4.

Stroke predictor. We adopt a DETR-style architecture similar to PaintTransformer [33], which outputs a set of candidate strokes for each image region. Each stroke prediction is represented as $(c_p, x_{\text{shift}}, y_{\text{shift}}, scr_r)$, where $x_{\text{shift}}, y_{\text{shift}}$ specify the placement offset, and $scr_r \in (0, 1)$ is a ranking score indicating the relative drawing order. For training, we first redefine a matching loss that aligns each predicted stroke with a ground-truth stroke under optimal assignment:

$$\mathcal{L}_{\text{match}} = \min_{\sigma} \sum_i \left(\lambda_{L1} \|P_i^- - \hat{P}_{\sigma(i)}^-\|_1 + \lambda_{\text{cos}} \text{Cosine}(P_i^-, \hat{P}_{\sigma(i)}^-) + \lambda_D \text{BCE}(d_i, \hat{d}_{\sigma(i)}) \right). \quad (16)$$

where $P^- = (c_p, x_{\text{shift}}, y_{\text{shift}})$ excludes the ranking score, σ is the optimal bipartite matching, and $d \in \{0, 1\}$ indicates stroke presence.

However, set-based prediction does not impose any ordering, which often leads to incoherent overlaps when strokes are drawn directly, as shown in Fig 5. To address this, we introduce a ranking loss. Suppose the ground truth provides a sequence of strokes indexed as $\{1, 2, \dots, vs\}$ in their correct drawing order, where a smaller index means the stroke should be painted earlier. For each valid sequence, the predictor outputs $\{scr_{r,u}\}_{u=1}^{vs}$, we regularize the predicted scores:

$$\mathcal{L}_{\text{rank}} = \sum_{i < j} \max\left(0, scr_{r,\sigma(i)} - scr_{r,\sigma(j)} + (j - i) \cdot \text{margin}\right), \quad (17)$$

where i and j are ground-truth stroke indices. This loss penalizes cases where a stroke that should appear earlier (smaller i) is assigned a higher or nearly equal score compared to a later stroke (larger j). The margin term



Fig. 6. Examples of the collected strokes.

requires a minimum separation proportional to the index gap, preventing strokes that are far apart in the sequence from collapsing into nearly identical scores.

The overall training objective is

$$\mathcal{L}_{\text{total}} = \lambda_m \mathcal{L}_{\text{match}} + \lambda_r \mathcal{L}_{\text{rank}}, \quad (18)$$

Composition. Once trained, the predictor outputs both stroke parameters and their inferred order. Strokes are then generated by StrokeDiff and rendered sequentially layer by layer, producing a coherent painting with reduced overlap artifacts and more natural temporal structure.

4 Experiments

4.1 Dataset

To more closely mimic human painting behavior, we curated a dataset of 520 unique oil-painting strokes collected from a professional artist. Each stroke was drawn freely on a 20×26 grid canvas, as shown in Fig. 6, which illustrates the raw scanned sheet. Individual strokes were then cropped from the canvas and standardized to 295×295 pixels. We divided the dataset into 470 strokes for training and 50 for testing. To mitigate the limited sample size, we applied a series of preprocessing and augmentation steps, including background removal, color normalization, flipping, and rotation. This process expanded the dataset to 9,400 training images and 1,000 test image. The dataset is publicly available at DOI: [10.21227/t6bd-cs26](https://doi.org/10.21227/t6bd-cs26) to support further research.

4.2 Implementing details

StrokeDiff is trained on a dataset of 9,400 augmented brushstroke images. For each training instance, we randomly sample 32 additional strokes from the dataset as visual priors, resulting in 300,800 training pairs. The model builds upon Stable Diffusion v1_5 and generates outputs at a resolution of 512×512 . We use the original noise schedule from Stable Diffusion, where $\bar{\alpha}_t = \prod_{i=0}^t (1 - \beta_i)$, with β_t linearly interpolated between $\sqrt{0.00085}$ and $\sqrt{0.012}$. The prior upper bound Υ for η is set to 0.5. Training is conducted using PyTorch 1.9.0. The model is first trained for 4 epochs without parameter conditioning, followed by 5 epochs of fine-tuning with conditional inputs.

The stroke predictor operates on input canvases of size 32×32 and predicts up to 8 strokes per image. The matching loss weight vector $\lambda_m = [5, 10, 10]$ corresponds to the L_1 , cosine, and decision loss terms, respectively. $\lambda_r = 5$, and margin value is 0.125. The model was trained for 220 epochs.

Table 1. Comparison of diffusion-based approaches for stroke generation, all trained on SD1.5. n . and r . denote the average number of closed regions per stroke and the ratio of region area to the full image, respectively. Δ indicates the change relative to the dataset-only baseline (FID = 47.3, computed between train and test; CRD (n./r.) = 1.09 (0.188)).

Method	FID ↓	Δ	CRD (n./r.) ↓	Δ
INS $b=0.3$ [5]	273	+225	48.51 (0.675)	+47. (+0.49)
INS $b=0.6$ [5]	251	+203	44.14 (0.732)	+43. (+0.54)
SD1.5_LoRA[15]	285	+237	88.13 (0.760)	+87. (+0.57)
SmR (ours)	54	+6	1.24 (0.254)	+0.15 (+0.07)

Table 2. Comparison with prior stroke generation methods for controllable generation, all trained on our dataset. \dagger StrokeGAN and Stylized are conditioned on stroke parameters during training. RobPaint does not support conditional generation, so we evaluate it using its reconstruction outputs.

Model	Size	LPIPS ↓	MSE ↓	FID ↓
StrokeGAN [53]	$64 \times 64 \times 3$	0.285	0.064	245
Stylized [61]	$128 \times 128 \times 3$	0.242	0.036	273
RobPaint [1] \dagger	$64 \times 32 \times 1$	0.234	0.085	322
StrokeDiff	$512 \times 512 \times 3$	0.232	0.031	52

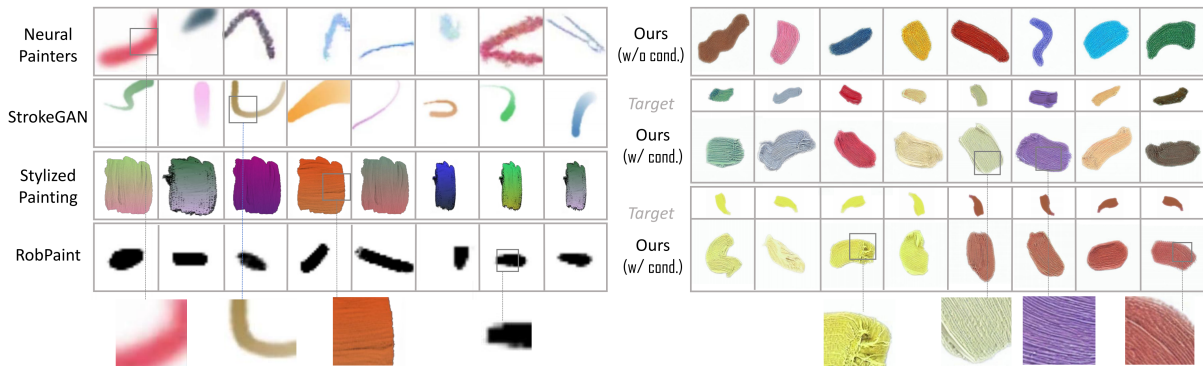


Fig. 7. Qualitative comparison with other approaches: 1) Neural Painters [36], using VAE and GAN trained on synthetic MyPaint strokes; 2) StrokeGAN [53], a GAN trained on fourth-order Bézier curves; 3) Template strokes [33, 47, 50, 61], taken from a widely used set of shapes commonly adopted in SBR; and 4) RobPaint [1], a VAE trained with human grayscale strokes. Our method generates clearer strokes while preserving brush textures.

4.3 Impact of Smooth Regularization on Stroke Generation

4.3.1 Evaluating generalization in few-shot diffusion. Table 1 reports quantitative results comparing SmR with representative low-resource training strategies for unconditional stroke generation, including noise schedule adjustment and LoRA-based fine-tuning. Evaluation is conducted using FID [11], as well as a structure-sensitive metric we introduce, Closed Region Detection (CRD). The motivation for CRD is that failures in stroke generation often manifest as either fragmented artifacts resembling multiple small brush-like patches or, conversely, as large blobs where strokes merge into indistinct masses. To capture these structural failures, CRD measures (i) the number of closed regions per image and (ii) the proportion of stroke area relative to the canvas. Both are computed via connected component analysis in OpenCV. For noise scheduling, we adapt *strategy 2* from INS [5], modifying the scaling factor b in the forward noise term to mitigate its counteracting effect. Setting $b = 1$ corresponds to the default schedule. We evaluate b values of 0.3 and 0.6. Although LoRA [15] was originally proposed for efficient fine-tuning, we include it as a strong low-data baseline due to its favorable parameter efficiency. Despite using only 470 hand-drawn strokes, SmR achieves a significantly lower FID. Both INS-based noise scheduling and LoRA fail to prevent structure collapse or mode proliferation: the number of detected regions is significantly overestimated, and FID remains high (qualitative examples can be seen in Fig. 11 columns 2–4).



Fig. 8. Qualitative comparison of paintings produced by different stroke-based rendering pipelines: Diffvg [29], Learn2Paint [22], Stylized [61], PT [33], and StrokeGAN [53]. The figure illustrates how different stroke generation strategies affect texture appearance, stroke irregularity, and layering behavior in the final compositions. Zoom in to see differences.

4.3.2 Quantitative comparison with stroke generation methods. We further evaluate SmR in the context of controllable stroke generation, comparing against prior work including StrokeGAN [53], Stylized [61], and RobPaint [1]. Table 2 reports LPIPS [60], MSE, and FID scores, where our model applied with SmR outperforms all methods across all metrics. We note that stroke data, unlike natural images, often exhibits lower perceptual and pixel-level variance, which limits the sensitivity of LPIPS and MSE in distinguishing structural quality. We found FID remains more discriminative in capturing distributional mismatch in the experiments, and SmR achieves the lowest FID, indicating that its outputs better align with the training data distribution. Qualitative results are shown in Appendix.

4.3.3 Qualitative comparison of strokes in other methods. Fig. 7 shows qualitative results from several representative stroke generation models. Neural Painters [36] and StrokeGAN [53] produce smooth outputs but show limited texture fidelity. Template-based approaches exhibit high pixel accuracy but constrained variability, while RobPaint [1] generates more organic strokes but lacks color expressiveness due to grayscale training. In comparison, StrokeDiff demonstrates both unconditional and conditional generation capabilities: the unconditional one-shot setting outputs feature diverse, textured strokes with clear structural integrity. When conditioned on specific parameters, the model accurately matches the targets in both shape and appearance. The final row shows augmented targets used in training, highlighting the model’s capacity to capture a wide range of brushstroke styles.

4.4 StrokeDiff in Downstream Painting Tasks

We next evaluate the rendering stage described in Section 3.4, focusing on the quality of complete paintings. We compare our method against representative approaches, including Diffvg [29], Learn2Paint [22], PaintTransformer

Table 3. CLIP score comparison across different methods. Ori. denotes reference images.

Method	Ori.	Diffvg	L2P	Styl.	PT	SGAN	Ours
CLIP Score	cap.1	0.125	0.1704	0.1879	0.1981	0.1751	0.1886
	cap.2	0.117	0.1757	0.2004	0.2059	0.1896	0.2019
	cap.3	0.106	0.1710	0.1970	0.2079	0.1901	0.1960
	cap.4	0.131	0.1950	0.2254	0.2294	0.2079	0.2097

Table 4. Human evaluation on painting quality (1–5 scale).

	Diffvg	L2P	Stylized	PT	S.GAN	Ours
Style	3.21	3.09	3.35	3.18	3.26	3.38
Aesthetic	2.87	2.50	3.00	2.76	3.11	3.38
Texture	2.84	2.39	3.18	2.79	2.94	3.50
Content	4.35	4.12	3.37	3.48	3.39	2.59
Total	3.32	3.03	3.24	3.05	3.17	3.21

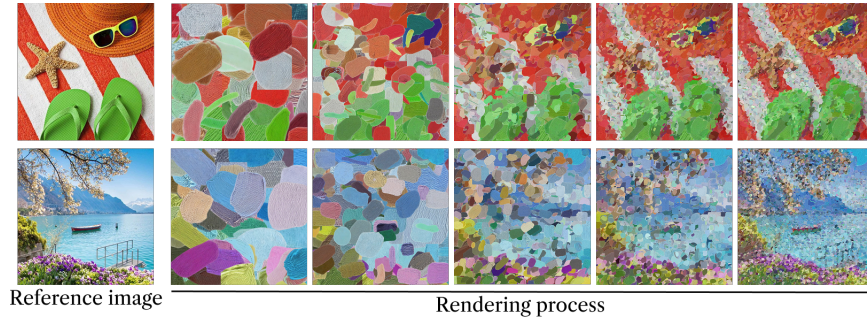


Fig. 9. Intermediate canvases in the rendering process.

(PT) [33], Stylized [61], and StrokeGAN [53]. These methods span differentiable vector graphics, reinforcement learning, feed-forward prediction, and GAN-based stroke generation.

4.4.1 Qualitative evaluation of paintings. Fig. 8 compares the painting results produced by different stroke-based rendering approaches. Diffvg and Learn2Paint focus on accurate pixel-level reconstruction, resulting in images that closely follow the reference but rely on relatively uniform and geometry-driven stroke patterns. Stylized and StrokeGAN introduce higher shape variability, yet their strokes often exhibit simplified textures or less consistent layering behavior. Our method adopts a different emphasis by modeling strokes as texture-rich and irregular visual primitives. As a result, the rendered paintings show more pronounced stroke texture, clearer layering structure, and a visual appearance that aligns more closely with the characteristics of oil painting. Fig. 9 further illustrates how such stroke-level properties accumulate during the sequential rendering process.

4.4.2 Quantitative evaluation of paintings. Table 3 reports semantic alignment measured by CLIP score. We evaluate each method on five images using four descriptive captions: “an oil painting made by a human”, “a brushstroke oil painting”, “a textured oil painting”, and “a stylized oil painting with strong brushstroke texture made by a human”. Results show that our approach reaches a similar score to Stylized on the first caption. On the remaining three captions, which emphasize brushstroke texture and stylization, our method consistently surpasses all alternatives. These improvements suggest that StrokeDiff better aligns with human-oriented descriptions of oil painting, especially in aspects related to stroke quality and artistic expression.

4.4.3 User Study. Following [52], we conducted a human evaluation with 51 participants, including 26 with formal art backgrounds and 25 without. Participants rated each method on four criteria: *oil painting style*, *aesthetic value*, *texture*, and *content retention*. As shown in Table 4, our approach earned the highest ratings for style, aesthetics, and texture. However, its emphasis on artistic expression led to a lower content retention score, suggesting a trade-off between fidelity and stylization. The questionnaire is provided in Appendix.

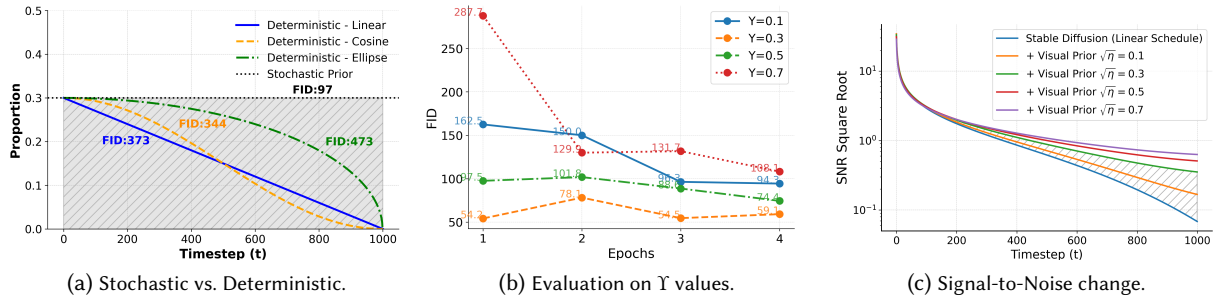


Fig. 10. Ablation results. (a) Injection trend of stochastic and deterministic prior; (b) FID across training epochs for different Υ values; (c) SNR changes. We take the square root of standard SNR.

Table 5. Evaluation on different numbers of target-prior pairs for each data sample. The left and right groups correspond to cases where Υ is set to 0.3 and 0.5.

# Multiple Pairs →	10	20	32	10	20	32
FID	148.6	91.6	54.2	108	97.5	74.4

4.5 Ablation studies

4.5.1 Analyzing the Role of Visual Prior Injection.

Evaluation on stochastic visual prior. We compare our stochastic prior injection strategy with deterministic alternatives. In our method, the injection factor is randomly sampled and remains step-independent, while deterministic priors follow a fixed schedule across time—analogue to noise schedules in standard diffusion models (e.g., linear, cosine, or scaled cosine schedules), commonly used for controlling the diffusion strength via predefined α_t or β_t curves. We test several such deterministic variants, including linear, cosine, and ellipse-shaped prior weights. As shown in Fig. 10a, our approach achieves a significantly lower FID, as it prevents the model from propagating fixed information, enabling the model to better adapt to stroke variations and learn a broader sample distribution. The *gray-shaded* area in the figure represents the range of possible prior values introduced by the stochastic method, highlighting that it is no longer a fixed trajectory.

Evaluation on prior upper bound. We evaluated different values of the prior upper bound Υ . As shown in Fig. 10b, the model can converge across four tested values, with clear early-stage convergence at $\Upsilon = 0.3$ and 0.5, particularly at 0.3, where the model stabilized within the first epoch. In our other experiments, we found that $\Upsilon = 0.5$ performs comparably to $\Upsilon = 0.3$ after conditioning training, but was more robust in low-data scenarios. Therefore, setting $\Upsilon = 0.3$ accelerates training when data is sufficient, while a higher upper bound provides stronger guidance in low-data settings. Table 5 shows results for different numbers of priors matches per sample, where larger Υ is beneficial when fewer pairs are available. We did not test beyond 32 pairs, as this was already sufficient to produce high-quality strokes.

Effect on SNR dynamics. Although our method does not explicitly perform noise scheduling, injecting visual priors during the forward process inherently modifies the signal-to-noise ratio (SNR). This connection offers a complementary perspective on how SmR improves training. Fig. 10c illustrates the expected SNR trajectory when $\sqrt{\eta} = 0.3$ is applied uniformly across timesteps, treating the prior as part of the signal (green curve). In practice,

Noise Scheduling	×	b=0.3	b=0.6		✓	✓	✓	✓	✓	✓	✓	✓
Visual Prior	×	×	×		✓	✓	✓	×	✓	×	×	✓
+addition method (Det./Sto.)	×	×	×	LoRA	Det.-ellipse	Det.-linear	Det.-cosine	×	Sto.	Sto.	Sto.	Sto.
+multiple pairs	×	×	×		✓	✓	✓	×	×	×	✓	✓
upper bound	-	-	-		-	-	-	0.5	0.5	0.5	0.5	0.3
FID	323	273	251		473	344	373	336	164	147	97	54

Fig. 11. Example results from ablation experiments. Since the default prior-sample pairs are 32, all "w/o multi-pairs" settings were trained for 32 epochs to match the total number of updates, while other settings were trained for 1 epoch. *Det.* and *Sto.* denote deterministic and stochastic prior injection methods. Although LoRA is not part of our ablation, we include its results in the fourth column for qualitative comparison.

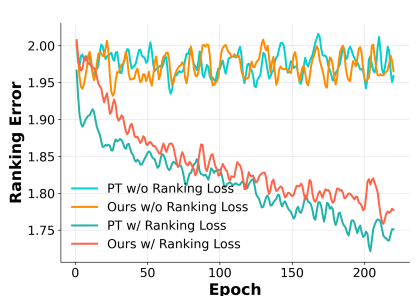


Fig. 12. Rank error w/ and w/o Ranking Loss. For the method w/o Ranking Loss, src_r is replaced by predicted index \times margin.

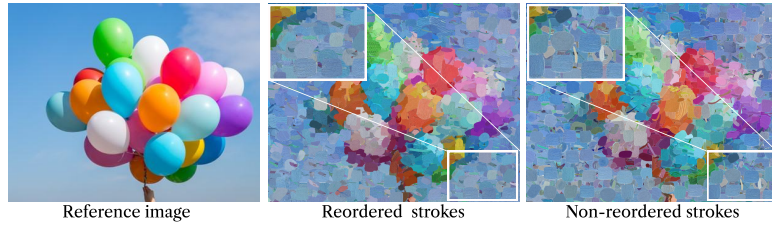


Fig. 13. Paints w/ and w/o reordered strokes using predicted rank scores.

due to stochastic injection, the actual SNR fluctuates within the shaded band, consistently higher than that of standard Stable Diffusion.

Augmentation effect. To isolate the augmentation effect of SmR, we further test a degenerate case where the prior x_s is replaced with x_0 (ground truth). As shown in Fig. 11 (third-to-last column), even without introducing new information, this variant significantly reduces FID, suggesting that SmR acts as an effective training-time regularizer beyond data augmentation. Exploring this property in other domains is an interesting direction for future work.

4.5.2 Ablation on ranking loss. We assessed the stroke predictor's ability to maintain a consistent rendering order by measuring sequence error between predicted and ground-truth stroke orders, with and without Ranking Loss. As shown in Fig. 12, without the Ranking Loss, the model's set-based prediction approach leads to a completely unordered sequence, which affects the overall coherence of the painting. With the Ranking Loss, the stroke order progressively aligns with the correct sequence. We also tested this approach on PT [33] and observed similar

Table 6. Results on Paint-by-Example with subsets of Open-Images.

Method	8% Open-Images			1% Open-Images		
	FID ↓	QS ↑	CLIP ↑	FID ↓	QS ↑	CLIP ↑
Paint-by-Example	11.667	73.254	74.120	27.421	27.473	58.827
+ SmR (x_0)	11.467	73.981	73.544	26.858	31.148	57.179

improvements. Fig.13 further illustrates that without reordering, strokes exhibit noticeable layering artifacts, whereas reordering produces a more cohesive blending.

4.6 Generality Beyond Stroke Generation

To examine whether Smooth Regularization can benefit domains other than stroke synthesis, we conducted a preliminary test on the inpainting task Paint-by-Example [57], which provides a complete training and evaluation framework. Following the same training protocol, we applied a degenerate form of SmR where the visual prior was set to the input x_0 . Both the baseline and the SmR-augmented models were trained on subsets of the Open-Images [27] dataset, using either 8% or 1% of the training data. Table 6 summarizes the results. While performance at the 8% data level is broadly comparable, SmR yields modest gains in the extremely low-data regime (1%), with lower FID and higher quality scores. These preliminary results suggest that SmR may act as a useful training-time regularizer beyond stroke generation, although broader validation across diverse tasks remains an open direction for future work.

5 Discussion

5.1 Potential application scenarios

Beyond the scope of our current experiments, it is worth considering how stroke-level generation could be applied in related domains.

Robotic painting. One natural direction is robotic painting, where diffusion-based strokes may be mapped to robotic arm trajectories in order to reproduce brush-like appearances with greater fidelity. Recent systems such as FRIDA [41] and COFRIDA [43] have already shown the feasibility of combining generative models with robotic painting, and stroke-level synthesis could further enrich this process by providing more diverse and textured visual units.

Creative support tools. CSTs are interactive systems that assist the creative process by providing real-time, controllable enhancements while keeping the user in primary creative control. In this context, the texture expressiveness of our strokes could be extended to serve as rendering units embedded in digital painting toolchains, such as styluses or touchscreen brushes. This idea is related to Diffusion Texture Painting [14], which demonstrated how diffusion models can enrich user input with textured feedback. StrokeDiff differs in that it focuses on stroke-level synthesis, and could therefore be explored in future as a complementary component for producing painterly, layered brush effects in educational or creative software.

2.5D printing. Advances in 2.5D and relief printing technologies (e.g., Canon’s surface-relief printing) have made it possible to reproduce tactile qualities in artworks. However, existing pipelines typically rely on heuristic mappings from RGB values to height maps, which may fail to capture fine brush textures. Because our strokes explicitly encode layered and textured appearances, they could be converted into printable height fields that preserve the physical feel of oil painting. Such an application would expand the use of stroke synthesis from visual rendering to tangible reproduction.

5.2 Evaluation Challenges in AI-Based Painting

In our user study, participants were asked to rate “From the photograph to the painting, how well is the content applied in the artwork?”. Compared with style, aesthetics, and texture, the scores for this content-related question were noticeably lower. This raises an important question: does a lower content score necessarily imply weaker performance, or does it instead reflect the tension between abstraction and fidelity that is central to non-photorealistic rendering? In our case, the generated strokes do not alter object presence or layout, but reinterpret the same content with varying degrees of abstraction, which makes the notion of “content preservation” itself somewhat ambiguous. From one viewpoint, reduced fidelity is a shortcoming; from another, it is an expected property of artistic stylization. This ambiguity points to a broader issue in the evaluation of AI-based painting systems. Much of the existing work on aesthetic assessment [24] or art criticism [2] focuses on finished artworks, which often focus on finished masterpieces or historical paintings, differing substantially from process-oriented generative painting. Consequently, there remains a lack of comprehensive benchmarks that can assess painting systems across multiple dimensions, such as semantic coherence, abstraction level, stroke expressiveness, and stylistic intent, depending on task requirements. Widely-used image metrics, including FID or CLIP-based similarity, primarily capture distributional alignment or coarse semantic correspondence, but are insensitive to non-rigid, perceptual qualities central to artistic rendering. Recent evaluation protocols for generative tasks have begun to incorporate large multimodal language models as flexible judges, for example through GPT-based or VQA-style assessments in benchmarks such as T2I-CompBench++ [20], as well as through general-purpose VLMs including the LLaVA family [31] and Qwen2-VL [51]. These models enable evaluation along qualitative dimensions that are difficult to formalize numerically. While still imperfect, MLLM-based evaluation offers a promising complementary direction for assessing AI painting systems beyond traditional pixel- or embedding-level metrics.

6 Limitations and future work

6.1 Rendering pipeline

In this work we adopted a PaintTransformer-style predictor as the downstream rendering pipeline, primarily because its feed-forward design is computationally efficient. However, this design choice also inherits limitations that are common to similar approaches such as Learn2Paint and StrokeGAN. In particular, the grid-based layer-wise rendering strategy divides the canvas into $2^k \times 2^k$ patches at k -th layer, leading to strokes that are locally constrained and often uniform in size. This behavior differs from human painting practices, where artists naturally vary stroke length, orientation, and continuity depending on the region and intended effect. An alternative direction would be to integrate StrokeDiff into frameworks such as Diffvg, where stroke placement is jointly optimized over the canvas. In principle, such integration could allow longer strokes that align with object contours and reduce the grid artifact, although it would require adjustments in stroke parameterization and pipeline integration.

6.2 Style diversity and generalization

StrokeDiff is particularly suited to texture-rich colored painting styles such as oil painting, where irregular boundaries and layered pigments are central to the visual effect. Other domains, such as sketch strokes, have very different visual characteristics: they are typically sparse, monochromatic, and lack continuous texture, which suggests that vector-domain modeling with rasterization might be a more natural choice than diffusion-based texture synthesis. For other colored media, including watercolor and ink wash, we have not yet attempted generalization. The main limitation here is the lack of domain-specific datasets, which makes it difficult to capture phenomena such as transparency, pigment blending, and negative-space effects. To explore this direction, we are currently constructing a dataset of 1,008 ink-style brushstrokes. This resource will allow us to examine

stroke generation in a medium with different physical properties and may inform future adaptations of stroke parameterization and rendering rules.

6.3 Generalization of SmR

Although we included a preliminary experiment in Section 4.6 using an inpainting framework, this alone is not sufficient to demonstrate that SmR generalizes across domains. Whether it can serve as a general-purpose regularization strategy remains to be established through broader validation. Nevertheless, for tasks where data collection is difficult or where the goal is to generate fundamental primitives as building blocks, SmR could have potential value and merits further investigation.

7 Conclusion

This work explored the problem of brushstroke generation under limited data and introduced StrokeDiff with Smooth Regularization as a data-efficient diffusion framework. The results show that stroke-level modeling can be both structurally diverse and stylistically expressive, and that such primitives can be composed into convincing paintings. More broadly, this study illustrates how generative models can contribute to non-photorealistic rendering when adapted to domain-specific primitives. Future work may extend this direction to other artistic media, and explore more comprehensive evaluation protocols that account for both abstraction and fidelity.

Acknowledgments

This work is supported by the Research Grants Council of Hong Kong under the Theme-based Research Scheme (T45-205/21-N).

References

- [1] Ardavan Bidgoli, Manuel Ladrón De Guevara, Cinnie Hsiung, Jean Oh, and Eunsu Kang. 2020. Artistic style in robotic painting; a machine learning approach to learning brushstroke from human artists. In *2020 29th IEEE International Conference on Robot and Human Interactive Communication (RO-MAN)*. IEEE, 412–418.
- [2] Yi Bin, Wenhao Shi, Yujuan Ding, Zhiqiang Hu, Zheng Wang, Yang Yang, See-Kiong Ng, and Heng Tao Shen. 2024. Gallerygpt: Analyzing paintings with large multimodal models. In *Proceedings of the 32nd ACM International Conference on Multimedia*. 7734–7743.
- [3] Eva Cetinic and James She. 2022. Understanding and creating art with AI: Review and outlook. *ACM transactions on multimedia computing, communications, and applications (TOMM)* 18, 2 (2022), 1–22.
- [4] Lawrence Chen, Peter Schaldenbrand, Tanmay Shankar, Lia Coleman, and Jean Oh. 2025. Spline-FRIDA: Towards Diverse, Humanlike Robot Painting Styles with a Sample-Efficient, Differentiable Brush Stroke Model. *IEEE Robotics and Automation Letters* (2025).
- [5] Ting Chen. 2023. On the importance of noise scheduling for diffusion models. *arXiv preprint arXiv:2301.10972* (2023).
- [6] Kevin Clark and Priyank Jaini. 2023. Text-to-Image Diffusion Models are Zero Shot Classifiers. In *Advances in Neural Information Processing Systems*, A. Oh, T. Naumann, A. Globerson, K. Saenko, M. Hardt, and S. Levine (Eds.), Vol. 36. Curran Associates, Inc., 58921–58937. https://proceedings.neurips.cc/paper_files/paper/2023/file/b87bdcf963cad3d0b265fcb78ae7d11e-Paper-Conference.pdf
- [7] Prafulla Dhariwal and Alexander Nichol. 2021. Diffusion models beat gans on image synthesis. *Advances in neural information processing systems* 34 (2021), 8780–8794.
- [8] Wenkai Dong, Song Xue, Xiaoyue Duan, and Shumin Han. 2023. Prompt tuning inversion for text-driven image editing using diffusion models. In *Proceedings of the IEEE/CVF International Conference on Computer Vision*. 7430–7440.
- [9] Jiatao Gu, Shuangfei Zhai, Yizhe Zhang, Miguel Angel Bautista, and Josh Susskind. 2022. f-dm: A multi-stage diffusion model via progressive signal transformation. *arXiv preprint arXiv:2210.04955* (2022).
- [10] Amir Hertz, Ron Mokady, Jay Tenenbaum, Kfir Aberman, Yael Pritch, and Daniel Cohen-Or. 2022. Prompt-to-prompt image editing with cross attention control.(2022). URL <https://arxiv.org/abs/2208.01626> (2022).
- [11] Martin Heusel, Hubert Ramsauer, Thomas Unterthiner, Bernhard Nessler, and Sepp Hochreiter. 2017. Gans trained by a two time-scale update rule converge to a local nash equilibrium. *Advances in neural information processing systems* 30 (2017).
- [12] Jonathan Ho and Tim Salimans. 2022. Classifier-free diffusion guidance. *arXiv preprint arXiv:2207.12598* (2022).
- [13] Emiel Hoogeboom, Jonathan Heek, and Tim Salimans. 2023. simple diffusion: End-to-end diffusion for high resolution images. In *International Conference on Machine Learning*. PMLR, 13213–13232.

- [14] Anita Hu, Nishkrit Desai, Hassan Abu Alhaija, Seung Wook Kim, and Maria Shugrina. 2024. Diffusion texture painting. In *ACM SIGGRAPH 2024 Conference Papers*. 1–12.
- [15] Edward J Hu, Yelong Shen, Phillip Wallis, Zeyuan Allen-Zhu, Yuanzhi Li, Shean Wang, Lu Wang, Weizhu Chen, et al. 2022. Lora: Low-rank adaptation of large language models. *ICLR* 1, 2 (2022), 3.
- [16] Hexiang Hu, Kelvin CK Chan, Yu-Chuan Su, Wenhu Chen, Yandong Li, Kihyuk Sohn, Yang Zhao, Xue Ben, Boqing Gong, William Cohen, et al. 2024. Instruct-imagen: Image generation with multi-modal instruction. In *Proceedings of the IEEE/CVF conference on computer vision and pattern recognition*. 4754–4763.
- [17] Juncheng Hu, Ximing Xing, Jing Zhang, and Qian Yu. 2024. VectorPainter: Advanced Stylized Vector Graphics Synthesis Using Stroke-Style Priors. *arXiv preprint arXiv:2405.02962* (2024).
- [18] Teng Hu, Ran Yi, Haokun Zhu, Liang Liu, Jinlong Peng, Yabiao Wang, Chengjie Wang, and Lizhuang Ma. 2023. Stroke-based Neural Painting and Stylization with Dynamically Predicted Painting Region. In *Proceedings of the 31st ACM International Conference on Multimedia*. 7470–7480.
- [19] Zhangli Hu, Ye Chen, Zhongyin Zhao, Jinfan Liu, Bilian Ke, and Bingbing Ni. 2024. Towards Artist-Like Painting Agents with Multi-Granularity Semantic Alignment. In *Proceedings of the 32nd ACM International Conference on Multimedia*. 10191–10199.
- [20] Kaiyi Huang, Chengqi Duan, Kaiyue Sun, Enze Xie, Zhenguo Li, and Xihui Liu. 2025. T2i-compbench++: An enhanced and comprehensive benchmark for compositional text-to-image generation. *IEEE Transactions on Pattern Analysis and Machine Intelligence* (2025).
- [21] Nisha Huang, Weiming Dong, Yuxin Zhang, Fan Tang, Ronghui Li, Chongyang Ma, Xiu Li, Tong-Yee Lee, and Changsheng Xu. 2025. CreativeSynth: Cross-Art-Attention for Artistic Image Synthesis With Multimodal Diffusion. *IEEE Transactions on Visualization and Computer Graphics* (2025).
- [22] Zhewei Huang, Wen Heng, and Shuchang Zhou. 2019. Learning to paint with model-based deep reinforcement learning. In *Proceedings of the IEEE/CVF international conference on computer vision*. 8709–8718.
- [23] Francisco Ibarrola, Tomas Lawton, and Kazjon Grace. 2023. A collaborative, interactive and context-aware drawing agent for co-creative design. *IEEE Transactions on Visualization and Computer Graphics* 30, 8 (2023), 5525–5537.
- [24] Xin Jin, Qianqian Qiao, Yi Lu, Huaye Wang, Heng Huang, Shan Gao, Jianfei Liu, and Rui Li. 2024. APDDv2: Aesthetics of Paintings and Drawings Dataset with Artist Labeled Scores and Comments. *arXiv preprint arXiv:2411.08545* 8, 9 (2024).
- [25] Dmytro Kotovenko, Matthias Wright, Arthur Heimbrecht, and Bjorn Ommer. 2021. Rethinking style transfer: From pixels to parameterized brushstrokes. In *Proceedings of the IEEE/CVF Conference on Computer Vision and Pattern Recognition*. 12196–12205.
- [26] Nupur Kumari, Bingliang Zhang, Richard Zhang, Eli Shechtman, and Jun-Yan Zhu. 2023. Multi-concept customization of text-to-image diffusion. In *Proceedings of the IEEE/CVF conference on computer vision and pattern recognition*. 1931–1941.
- [27] Alina Kuznetsova, Hassan Rom, Neil Alldrin, Jasper Uijlings, Ivan Krasin, Jordi Pont-Tuset, Shahab Kamali, Stefan Popov, Matteo Mallocci, Alexander Kolesnikov, et al. 2020. The open images dataset v4: Unified image classification, object detection, and visual relationship detection at scale. *International journal of computer vision* 128, 7 (2020), 1956–1981.
- [28] Jing Li, Jun Guo, M Shamim Hossain, and Ning Yu. 2025. Immersive Ink-and-Wash Landscape Design in Multimedia for Art Therapy. *ACM Transactions on Multimedia Computing, Communications and Applications* 21, 11 (2025), 1–26.
- [29] Tzu-Mao Li, Michal Lukáč, Michaël Gharbi, and Jonathan Ragan-Kelley. 2020. Differentiable vector graphics rasterization for editing and learning. *ACM Transactions on Graphics (TOG)* 39, 6 (2020), 1–15.
- [30] Shanchuan Lin, Bingchen Liu, Jiashi Li, and Xiao Yang. 2024. Common diffusion noise schedules and sample steps are flawed. In *Proceedings of the IEEE/CVF Winter Conference on Applications of Computer Vision*. 5404–5411.
- [31] Haotian Liu, Chunyuan Li, Qingyang Wu, and Yong Jae Lee. 2023. Visual instruction tuning. *Advances in neural information processing systems* 36 (2023), 34892–34916.
- [32] Ruoxue Liu, Linjiajie Fang, Wenjia Wang, and Bing-Yi Jing. 2024. D2R2: Diffusion-based Representation with Random Distance Matching for Tabular Few-shot Learning. In *Advances in Neural Information Processing Systems*, A. Globerson, L. Mackey, D. Belgrave, A. Fan, U. Paquet, J. Tomczak, and C. Zhang (Eds.), Vol. 37. Curran Associates, Inc., 36890–36913. https://proceedings.neurips.cc/paper_files/paper/2024/file/40eff1670d6b08bb1bda48b0c5f30110-Paper-Conference.pdf
- [33] Songhua Liu, Tianwei Lin, Dongliang He, Fu Li, Ruifeng Deng, Xin Li, Errui Ding, and Hao Wang. 2021. Paint transformer: Feed forward neural painting with stroke prediction. In *Proceedings of the IEEE/CVF international conference on computer vision*. 6598–6607.
- [34] Xiao-Chang Liu, Yu-Chen Wu, and Peter Hall. 2023. Painterly style transfer with learned brush strokes. *IEEE Transactions on Visualization and Computer Graphics* 30, 9 (2023), 6309–6320.
- [35] Ron Mokady, Amir Hertz, Kfir Aberman, Yael Pritch, and Daniel Cohen-Or. 2023. Null-text inversion for editing real images using guided diffusion models. In *Proceedings of the IEEE/CVF conference on computer vision and pattern recognition*. 6038–6047.
- [36] Reiichiro Nakano. 2019. Neural painters: A learned differentiable constraint for generating brushstroke paintings. *arXiv preprint arXiv:1904.08410* (2019).
- [37] Hyelin Nam, Jaemin Kim, Dohun Lee, and Jong Chul Ye. 2024. Optical-Flow Guided Prompt Optimization for Coherent Video Generation. *arXiv preprint arXiv:2411.15540* (2024).

- [38] Yunfang Niu, Lingxiang Wu, Yufeng Zhang, Yousong Zhu, Guibo Zhu, and Jinqiao Wang. 2024. Multi-Model Style-Aware Diffusion Learning for Semantic Image Synthesis. *ACM Transactions on Multimedia Computing, Communications and Applications* 20, 11 (2024), 1–21.
- [39] Robin Rombach, Andreas Blattmann, Dominik Lorenz, Patrick Esser, and Björn Ommer. 2022. High-resolution image synthesis with latent diffusion models. In *Proceedings of the IEEE/CVF conference on computer vision and pattern recognition*. 10684–10695.
- [40] Nataniel Ruiz, Yuanzhen Li, Varun Jampani, Yael Pritch, Michael Rubinstein, and Kfir Aberman. 2023. Dreambooth: Fine tuning text-to-image diffusion models for subject-driven generation. In *Proceedings of the IEEE/CVF conference on computer vision and pattern recognition*. 22500–22510.
- [41] Peter Schaldenbrand, James McCann, and Jean Oh. 2022. Frida: A collaborative robot painter with a differentiable, real2sim2real planning environment. *arXiv preprint arXiv:2210.00664* (2022).
- [42] Peter Schaldenbrand and Jean Oh. 2021. Content masked loss: Human-like brush stroke planning in a reinforcement learning painting agent. In *Proceedings of the AAAI conference on artificial intelligence*, Vol. 35. 505–512.
- [43] Peter Schaldenbrand, Gaurav Parmar, Jun-Yan Zhu, James McCann, and Jean Oh. 2024. Cofrida: Self-supervised fine-tuning for human-robot co-painting. In *2024 IEEE International Conference on Robotics and Automation (ICRA)*. IEEE, 2296–2302.
- [44] Jaskirat Singh, Cameron Smith, Jose Echevarria, and Liang Zheng. 2022. Intelli-Paint: Towards developing more human-intelligible painting agents. In *European Conference on Computer Vision*. Springer, 685–701.
- [45] Jaskirat Singh and Liang Zheng. 2021. Combining semantic guidance and deep reinforcement learning for generating human level paintings. In *Proceedings of the IEEE/CVF Conference on Computer Vision and Pattern Recognition*. 16387–16396.
- [46] Kihyuk Sohn, Nataniel Ruiz, Kimin Lee, Daniel Castro Chin, Irina Blok, Huiwen Chang, Jarred Barber, Lu Jiang, Glenn Entis, Yuanzhen Li, et al. 2023. Styledrop: Text-to-image generation in any style. *arXiv preprint arXiv:2306.00983* (2023).
- [47] Yiren Song, Shijie Huang, Chen Yao, Xiaojun Ye, Hai Ci, Jiaming Liu, Yuxuan Zhang, and Mike Zheng Shou. 2024. ProcessPainter: Learn Painting Process from Sequence Data. *arXiv preprint arXiv:2406.06062* (2024).
- [48] Yizhe Tang, Yue Wang, Teng Hu, Ran Yi, Xin Tan, Lizhuang Ma, Yu-Kun Lai, and Paul L Rosin. 2024. AttentionPainter: An Efficient and Adaptive Stroke Predictor for Scene Painting. *arXiv preprint arXiv:2410.16418* (2024).
- [49] Zhengyan Tong, Xuanhong Chen, Bingbing Ni, and Xiaohang Wang. 2021. Sketch generation with drawing process guided by vector flow and grayscale. In *Proceedings of the AAAI Conference on Artificial Intelligence*, Vol. 35. 609–616.
- [50] Zhengyan Tong, Xiaohang Wang, Shengchao Yuan, Xuanhong Chen, Junjie Wang, and Xiangzhong Fang. 2022. Im2Oil: Stroke-Based Oil Painting Rendering with Linearly Controllable Fineness Via Adaptive Sampling. In *Proceedings of the 30th ACM International Conference on Multimedia*. 1035–1046.
- [51] Peng Wang, Shuai Bai, Sinan Tan, Shijie Wang, Zhihao Fan, Jinze Bai, Keqin Chen, Xuejing Liu, Jialin Wang, Wenbin Ge, et al. 2024. Qwen2-vl: Enhancing vision-language model’s perception of the world at any resolution. *arXiv preprint arXiv:2409.12191* (2024).
- [52] Qian Wang, Hong-NingH Dai, Jinghua Yang, Cai Guo, Peter Childs, Maaik Kleinsmann, Yike Guo, and Pan Wang. 2024. Learning-based Artificial Intelligence Artwork: Methodology Taxonomy and Quality Evaluation. *Comput. Surveys* (2024).
- [53] Qian Wang, Cai Guo, Hong-Ning Dai, and Ping Li. 2023. Stroke-GAN Painter: Learning to paint artworks using stroke-style generative adversarial networks. *Computational Visual Media* 9, 4 (2023), 787–806.
- [54] Quan Wang, Sheng Li, Xinpeng Zhang, and Guorui Feng. 2022. Multi-granularity brushstrokes network for universal style transfer. *ACM Transactions on Multimedia Computing, Communications, and Applications (TOMM)* 18, 4 (2022), 1–17.
- [55] Yu-Ao Wang, James She, Troy TianYu Lin, and Kang Zhang. 2025. AI Visual Art History: An Art Movement with Expanded Artistic Horizon. *ACM Transactions on Multimedia Computing, Communications and Applications* 21, 7 (2025), 1–16.
- [56] Peizhi Yan, Rabab K Ward, Qiang Tang, and Shan Du. 2025. Neural 3D Face Shape Stylization Based on Single Style Template via Weakly Supervised Learning. *IEEE Transactions on Visualization and Computer Graphics* (2025).
- [57] Binxin Yang, Shuyang Gu, Bo Zhang, Ting Zhang, Xuejin Chen, Xiaoyan Sun, Dong Chen, and Fang Wen. 2023. Paint by example: Exemplar-based image editing with diffusion models. In *Proceedings of the IEEE/CVF conference on computer vision and pattern recognition*. 18381–18391.
- [58] Ruofeng Yang, Bo Jiang, Cheng Chen, Ruinan Jin, Baoxiang Wang, and Shuai Li. 2024. Few-Shot Diffusion Models Escape the Curse of Dimensionality. In *Advances in Neural Information Processing Systems*, A. Globerson, L. Mackey, D. Belgrave, A. Fan, U. Paquet, J. Tomczak, and C. Zhang (Eds.), Vol. 37. Curran Associates, Inc., 68528–68558. https://proceedings.neurips.cc/paper_files/paper/2024/file/7eb6233e02f7d9efbb84acd839a996fb-Paper-Conference.pdf
- [59] Xiaoyu Yue, Zidong Wang, Zeyu Lu, Shuyang Sun, Meng Wei, Wanli Ouyang, Lei Bai, and Luping Zhou. 2024. Diffusion models need visual priors for image generation. *arXiv preprint arXiv:2410.08531* (2024).
- [60] Richard Zhang, Phillip Isola, Alexei A Efros, Eli Shechtman, and Oliver Wang. 2018. The unreasonable effectiveness of deep features as a perceptual metric. In *Proceedings of the IEEE conference on computer vision and pattern recognition*. 586–595.
- [61] Zhengxia Zou, Tianyang Shi, Shuang Qiu, Yi Yuan, and Zhenwei Shi. 2021. Stylized neural painting. In *Proceedings of the IEEE/CVF Conference on Computer Vision and Pattern Recognition*. 15689–15698.

Online Appendix

Formula derivation of SmR

Proof of the Second Zonklar Equation

The forward process in diffusion models, such as DDPMs, describes how data transitions over time by progressively adding noise. The transitions between time steps can be represented as:

$$x_t = \sqrt{\alpha}x_{t-1} + \sqrt{1 - \alpha} \epsilon_{t-1}, \quad (19)$$

$$x_{t-1} = \sqrt{\alpha}x_{t-2} + \sqrt{1 - \alpha} \epsilon_{t-2}, \quad (20)$$

$$\vdots \quad (21)$$

$$x_2 = \sqrt{\alpha}x_1 + \sqrt{1 - \alpha} \epsilon_1, \quad (22)$$

$$x_1 = \sqrt{\alpha}x_0 + \sqrt{1 - \alpha} \epsilon_0. \quad (23)$$

We introduce an additional visual prior x_s into various stages of the diffusion process, allowing semantic information to guide the process, making the modified forward process partially dependent on this visual prior:

$$x'_t = x_t + \sqrt{1 - \bar{\alpha}_t} \sqrt{\eta} x_s - \sqrt{1 - \bar{\alpha}_t} \sqrt{\eta} \cdot \epsilon_t^*, \quad (24)$$

$$x'_{t-1} = x_{t-1} + \sqrt{1 - \bar{\alpha}_{t-1}} \sqrt{\eta} x_s - \sqrt{1 - \bar{\alpha}_{t-1}} \sqrt{\eta} \cdot \epsilon_{t-1}^*, \quad (25)$$

$$\vdots \quad (26)$$

Where $\epsilon^* \sim \mathcal{N}(0, I)$ is independently sampled noise, and $\sqrt{\eta} \sim \text{Uni}[0, 0.5]$ is a scaling factor. x_s is added directly at each timestep, but it does not evolve or propagate iteratively through the sequence. Therefore, x'_t is derived from x_t and is implicitly related to x'_{t-1} .

Proof: The Sequence $X = \{x_0, x'_1, x'_2, \dots, x'_t\}$ is Markovian

To utilize Bayes' theorem for calculating the new sampling distribution, $q(x'_t|x'_{t-1}, x_0)$ and $q(x'_t|x'_{t-1})$ must be equivalent. Therefore, it is necessary to prove that the sequence $X = \{x_0, x'_1, x'_2, \dots, x'_t\}$ is Markovian.

The sequence dependencies are defined as:

$$x_{t-1} \rightarrow x'_{t-1} = f(x_{t-1}, \epsilon_{t-1}^*, x_s), \quad x_{t-1} \rightarrow x_t = g(x_{t-1}, \epsilon_{t-1}), \quad x_t \rightarrow x'_t = h(x_t, \epsilon_t^*, x_s), \quad (27)$$

x_s is provided as a fixed visual prior and shared across all steps. Thus, x'_t depends only on x_t , which depends only on x_{t-1} , and x'_{t-1} is derived directly from x_{t-1} , encapsulating all relevant information from x_{t-1} . Since x'_t depends on x'_{t-1} only through the intermediate state x_t , any dependency on earlier states (x'_{t-2}, x_{t-2}, \dots) is mediated by x'_{t-1} . Each Gaussian noise term ($\epsilon_{t-1}^*, \epsilon_{t-1}, \epsilon_t^*$) is independently sampled. This ensures there are no hidden dependencies between x'_t and earlier states beyond x'_{t-1} .

Given the encapsulation of information and the independence of noise, the conditional dependency simplifies to:

$$P(x'_t|x_0, x'_1, \dots, x'_{t-1}) = P(x'_t|x'_{t-1}).$$

Thus, the sequence $X = \{x_0, x'_1, x'_2, \dots, x'_t\}$ satisfies the Markov property.

New sampling distribution

x'_t and x'_{t-1} can be expressed as follows:

$$x'_t = \sqrt{\bar{\alpha}_t} x_0 + \sqrt{1 - \bar{\alpha}_t} \sqrt{\eta} x_s + \sqrt{1 - \bar{\alpha}_t} \bar{\epsilon}_t - \sqrt{1 - \bar{\alpha}_t} \sqrt{\eta} \epsilon_t^* \quad (28)$$

$$x'_{t-1} = \sqrt{\bar{\alpha}_{t-1}} x_0 + \sqrt{1 - \bar{\alpha}_{t-1}} \sqrt{\eta} x_s + \sqrt{1 - \bar{\alpha}_{t-1}} \bar{\epsilon}_{t-1} - \sqrt{1 - \bar{\alpha}_{t-1}} \sqrt{\eta} \epsilon_{t-1}^* \quad (29)$$

$$x'_t = x_t + \sqrt{1 - \bar{\alpha}_t} \sqrt{\eta} x_s - \sqrt{1 - \bar{\alpha}_t} \sqrt{\eta} \cdot \epsilon_t^* \quad (30)$$

$$= \sqrt{\bar{\alpha}_t} x_{t-1} + \sqrt{1 - \bar{\alpha}_t} \sqrt{\eta} x_s + \sqrt{1 - \bar{\alpha}_t} \epsilon_{t-1} - \sqrt{1 - \bar{\alpha}_t} \sqrt{\eta} \epsilon_t^* \quad (31)$$

$$= \sqrt{\bar{\alpha}_t} \left(x'_{t-1} - \sqrt{1 - \bar{\alpha}_{t-1}} \sqrt{\eta} x_s + \sqrt{1 - \bar{\alpha}_{t-1}} \sqrt{\eta} \epsilon_{t-1}^* \right) \quad (32)$$

$$+ \sqrt{1 - \bar{\alpha}_t} \epsilon_{t-1} - \sqrt{1 - \bar{\alpha}_t} \sqrt{\eta} \epsilon_t^* + \sqrt{1 - \bar{\alpha}_t} \sqrt{\eta} x_s$$

$$= \sqrt{\bar{\alpha}_t} x'_{t-1} + \left(\sqrt{1 - \bar{\alpha}_t} - \sqrt{\bar{\alpha}_t} \sqrt{1 - \bar{\alpha}_{t-1}} \right) \sqrt{\eta} x_s \quad (33)$$

$$+ \sqrt{\bar{\alpha}_t} \sqrt{1 - \bar{\alpha}_{t-1}} \sqrt{\eta} \epsilon_{t-1}^* + \sqrt{1 - \bar{\alpha}_t} \epsilon_{t-1} - \sqrt{1 - \bar{\alpha}_t} \sqrt{\eta} \epsilon_t^*.$$

Therefore,

$$q(x'_t | x_0) = \mathcal{N} \left(x'_t; \sqrt{\bar{\alpha}_t} x_0 + \sqrt{1 - \bar{\alpha}_t} \sqrt{\eta} x_s, (1 + \eta) (1 - \bar{\alpha}_t) \mathbf{I} \right) \quad (34)$$

$$q(x'_{t-1} | x_0) = \mathcal{N} \left(x'_{t-1}; \sqrt{\bar{\alpha}_{t-1}} x_0 + \sqrt{1 - \bar{\alpha}_{t-1}} \sqrt{\eta} x_s, (1 + \eta) (1 - \bar{\alpha}_{t-1}) \mathbf{I} \right) \quad (35)$$

$$q(x'_t | x'_{t-1}) = \mathcal{N} \left(x'_t; \sqrt{\bar{\alpha}_t} x'_{t-1} + \left(\sqrt{1 - \bar{\alpha}_t} - \sqrt{\bar{\alpha}_t} \sqrt{1 - \bar{\alpha}_{t-1}} \right) \sqrt{\eta} x_s, ((1 + \alpha_t - 2\bar{\alpha}_t)\eta + 1 - \alpha_t) \mathbf{I} \right) \quad (36)$$

Bayes' theorem can calculate the posterior distribution:

$$\begin{aligned} q(x'_{t-1} | x'_t, x_0) &= \frac{q(x'_t | x'_{t-1}, x_0) q(x'_{t-1} | x_0)}{q(x'_t | x_0)} \\ &\propto \exp \left\{ -\frac{1}{2} \left[\frac{(x'_t - \sqrt{\bar{\alpha}_t} x'_{t-1} - (\sqrt{1 - \bar{\alpha}_t} - \sqrt{\bar{\alpha}_t} \sqrt{1 - \bar{\alpha}_{t-1}}) \sqrt{\eta} x_s)^2}{(1 + \alpha_t - 2\bar{\alpha}_t)\eta + 1 - \alpha_t} + \frac{(x'_{t-1} - \sqrt{\bar{\alpha}_{t-1}} x_0 - \sqrt{1 - \bar{\alpha}_{t-1}} \sqrt{\eta} x_s)^2}{(1 + \eta)(1 - \bar{\alpha}_{t-1})} - \frac{(x'_t - \sqrt{\bar{\alpha}_t} x_0 - \sqrt{1 - \bar{\alpha}_t} \sqrt{\eta} x_s)^2}{(1 + \eta)(1 - \alpha_t)} \right] \right\} \\ &= \exp \left\{ -\frac{1}{2} \left[\frac{\alpha_t x'^2_{t-1} - 2\sqrt{\bar{\alpha}_t} x'_t x'_{t-1} + 2\sqrt{\bar{\alpha}_t} (\sqrt{1 - \bar{\alpha}_t} - \sqrt{\bar{\alpha}_t} \sqrt{1 - \bar{\alpha}_{t-1}}) \sqrt{\eta} x_s x'_{t-1} + x'^2_{t-1} - 2\sqrt{\bar{\alpha}_{t-1}} x_0 x'_{t-1} - 2\sqrt{1 - \bar{\alpha}_{t-1}} \sqrt{\eta} x_s x'_{t-1} + \mathbf{C}(x'_t, x_0)}{(1 + \alpha_t - 2\bar{\alpha}_t)\eta + 1 - \alpha_t} \right] \right\} \\ &\propto \exp \left\{ -\frac{1}{2} \left[\frac{\alpha_t}{(1 + \alpha_t - 2\bar{\alpha}_t)\eta + 1 - \alpha_t} x'^2_{t-1} - 2 \frac{\sqrt{\bar{\alpha}_t} x'_t - \sqrt{\bar{\alpha}_t} (\sqrt{1 - \bar{\alpha}_t} - \sqrt{\bar{\alpha}_t} \sqrt{1 - \bar{\alpha}_{t-1}}) \sqrt{\eta} x_s}{(1 + \alpha_t - 2\bar{\alpha}_t)\eta + 1 - \alpha_t} x'_{t-1} + \frac{1}{(1 + \eta)(1 - \bar{\alpha}_{t-1})} x'^2_{t-1} - 2 \frac{\sqrt{\bar{\alpha}_{t-1}} x_0 + \sqrt{1 - \bar{\alpha}_{t-1}} \sqrt{\eta} x_s}{(1 + \eta)(1 - \bar{\alpha}_{t-1})} x'_{t-1} \right] \right\} \\ &= \exp \left\{ -\frac{1}{2} \left[\frac{1 - \bar{\alpha}_t + (1 + 2\alpha_t - 3\bar{\alpha}_t)\eta}{((1 + \alpha_t - 2\bar{\alpha}_t)\eta + 1 - \alpha_t)(1 + \eta)(1 - \bar{\alpha}_{t-1})} x'^2_{t-1} - 2 \left[\frac{\sqrt{\bar{\alpha}_t} x'_t - \sqrt{\bar{\alpha}_t} (\sqrt{1 - \bar{\alpha}_t} - \sqrt{\bar{\alpha}_t} \sqrt{1 - \bar{\alpha}_{t-1}}) \sqrt{\eta} x_s}{(1 + \alpha_t - 2\bar{\alpha}_t)\eta + 1 - \alpha_t} + \frac{\sqrt{\bar{\alpha}_{t-1}} x_0 + \sqrt{1 - \bar{\alpha}_{t-1}} \sqrt{\eta} x_s}{(1 + \eta)(1 - \bar{\alpha}_{t-1})} \right] x'_{t-1} \right] \right\} \\ &= \exp \left\{ -\frac{1}{2} \left[\frac{1}{\frac{(1 + \alpha_t - 2\bar{\alpha}_t)\eta + 1 - \alpha_t}{1 - \bar{\alpha}_t + (1 + 2\alpha_t - 3\bar{\alpha}_t)\eta} (1 + \eta)(1 - \bar{\alpha}_{t-1})} \left[x'^2_{t-1} - 2 \left[\dots \right] \right] ((1 + \alpha_t - 2\bar{\alpha}_t)\eta + 1 - \alpha_t) (1 + \eta)(1 - \bar{\alpha}_{t-1}) x'_{t-1} \right] \right\} \\ &= \exp \left\{ -\frac{1}{2} \left[\frac{1}{\frac{(1 + \alpha_t - 2\bar{\alpha}_t)\eta + 1 - \alpha_t}{1 - \bar{\alpha}_t + (1 + 2\alpha_t - 3\bar{\alpha}_t)\eta} (1 + \eta)(1 - \bar{\alpha}_{t-1})} \left[x'^2_{t-1} - 2 \frac{\sqrt{\bar{\alpha}_t} (1 - \bar{\alpha}_{t-1}) (1 + \eta) x'_t + \sqrt{\bar{\alpha}_{t-1}} ((1 - \alpha_t - 2\bar{\alpha}_t)\eta + 1 - \alpha_t) x_0 + f(\eta)}{1 - \bar{\alpha}_t + (1 + 2\alpha_t - 3\bar{\alpha}_t)\eta} x'_{t-1} \right] \right] \right\} \\ &\propto \mathcal{N} \left(x'_{t-1}; \underbrace{\frac{\sqrt{\bar{\alpha}_t} (1 - \bar{\alpha}_{t-1}) (1 + \eta) x'_t + \sqrt{\bar{\alpha}_{t-1}} ((1 - \alpha_t - 2\bar{\alpha}_t)\eta + 1 - \alpha_t) x_0 + f(\eta)}{1 - \bar{\alpha}_t + (1 + 2\alpha_t - 3\bar{\alpha}_t)\eta}}_{\mu_\eta(x'_t, x_0)}, \underbrace{\frac{((1 + \alpha_t - 2\bar{\alpha}_t)\eta + 1 - \alpha_t) (1 + \eta)(1 - \bar{\alpha}_{t-1})}{1 - \bar{\alpha}_t + (1 + 2\alpha_t - 3\bar{\alpha}_t)\eta}}_{\Sigma_\eta(\epsilon)} \mathbf{I} \right) \end{aligned}$$

The function $f(\eta)$ represents the independent term dependent on η , which can be expressed as:

$$f(\eta) = \sum_{k=1}^3 A_k \sqrt{\eta}^k, \quad (37)$$

where A_k are coefficients, determined by variables such as α_t , α_{t-1} , $\bar{\alpha}_t$, $\bar{\alpha}_{t-1}$, and x_s .

Model parametrization

The mean of $q(x'_{t-1}|x'_t, x_0)$ is:

$$\mu_q(x'_t, x_0) = \frac{\sqrt{\bar{\alpha}_t}(1 - \bar{\alpha}_{t-1})(1 + \eta)x'_t + \sqrt{\bar{\alpha}_{t-1}}((1 - \alpha_t - 2\bar{\alpha}_t)\eta + 1 - \alpha_t)x_0 + f(\eta)}{1 - \bar{\alpha}_t + (1 + 2\alpha_t - 3\bar{\alpha}_t)\eta} \quad (38)$$

From the derivation of the forward process $q(x'_t|x_0)$, we have an equivalent interpretation of x_0 expressed as:

$$x_0 = \frac{x_t - \sqrt{1 - \bar{\alpha}_t} \cdot \sqrt{1 - \eta} \cdot \epsilon - \sqrt{1 - \bar{\alpha}_t} \cdot \sqrt{\eta} \cdot x_s}{\sqrt{\bar{\alpha}_t}} \quad (39)$$

Let

$$\tau = \sqrt{1 + \eta}\epsilon + \sqrt{\eta}x_s, \quad (40)$$

the alternate parameterization for true denoising transition mean $\mu_q(x'_t, x_0)$ is:

$$\mu_q(x'_t, t) = \frac{\sqrt{\bar{\alpha}_t}(1 - \bar{\alpha}_{t-1})(1 + \eta)x'_t + \sqrt{\bar{\alpha}_{t-1}}((1 - \alpha_t - 2\bar{\alpha}_t)\eta + 1 - \alpha_t) \frac{x'_t - \sqrt{1 - \bar{\alpha}_t}\tau}{\sqrt{\bar{\alpha}_t}} + f(\eta)}{1 - \bar{\alpha}_t + (1 + 2\alpha_t - 3\bar{\alpha}_t)\eta} \quad (41)$$

$$= \frac{\sqrt{\bar{\alpha}_{t-1}}(1 - \bar{\alpha}_t)x'_t + (C_1)x'_t - \sqrt{\bar{\alpha}_{t-1}}\sqrt{1 - \bar{\alpha}_t}(1 - \alpha_t)\tau + (C_2)\tau + f(\eta)}{\sqrt{\bar{\alpha}_t}(1 - \bar{\alpha}_t + (1 + 2\alpha_t - 3\bar{\alpha}_t)\eta)}, \quad (42)$$

where C_1 and C_2 are also coefficients, with each term multiplied with η .

We parameterize $\hat{\tau}_\theta(x'_t, t)$ by neural networks that seek to predict both *underlying noise* and the *prior's effect* from noisy image x'_t . Then, the optimization problem simplifies to:

$$\mathbf{L}_\tau(\theta) = \mathbb{E} [\|\tau - \hat{\tau}_\theta(x'_t, t)\|^2]. \quad (43)$$

During inference, let $\eta = 0$, then:

$$\mu_q(x'_t, t) = \mu_q(x_t, t) \quad \text{in DDPM}, \quad (44)$$

$$\Sigma_q(t) = \Sigma_q(t) \quad \text{in DDPM} \quad (45)$$

We can still utilize the DDPM sampling formula to generate an image \hat{x} from Gaussian noise without requiring an additional visual prior x_s .

The proof of $\mu_q(x_t, t)$ in DDPM.

$$\mu_\theta(x_t, t) = \frac{\sqrt{\bar{\alpha}_t}(1 - \bar{\alpha}_{t-1})x_t + \sqrt{\bar{\alpha}_{t-1}}(1 - \alpha_t) \frac{x_t - \sqrt{1 - \bar{\alpha}_t}\epsilon}{\sqrt{\bar{\alpha}_t}}}{1 - \alpha_t} \quad (46)$$

$$= \frac{\sqrt{\bar{\alpha}_t}\sqrt{\bar{\alpha}_t}(1 - \bar{\alpha}_{t-1})x_t + \sqrt{\bar{\alpha}_{t-1}}(1 - \alpha_t)(x_t - \sqrt{1 - \bar{\alpha}_t}\epsilon)}{\sqrt{\bar{\alpha}_t}(1 - \alpha_t)} \quad (47)$$

$$= \frac{\alpha_t\sqrt{\bar{\alpha}_{t-1}}(1 - \bar{\alpha}_{t-1})x_t + \sqrt{\bar{\alpha}_{t-1}}(1 - \alpha_t)x_t - \sqrt{\bar{\alpha}_{t-1}}\sqrt{1 - \bar{\alpha}_t}(1 - \alpha_t)\epsilon}{\sqrt{\bar{\alpha}_t}(1 - \alpha_t)} \quad (48)$$

$$= \frac{\sqrt{\bar{\alpha}_{t-1}}(1 - \bar{\alpha}_t) - \sqrt{\bar{\alpha}_{t-1}}\sqrt{1 - \bar{\alpha}_t}(1 - \alpha_t)\epsilon}{\sqrt{\bar{\alpha}_t}(1 - \alpha_t)} \quad (49)$$

$$= \frac{1}{\sqrt{\bar{\alpha}_t}} \left(x_t - \frac{1 - \alpha_t}{\sqrt{1 - \bar{\alpha}_t}} \epsilon \right) \quad (50)$$

$\mu_q(x'_t, t)$ equals equation (31) when $\eta = 0$.

Dimension	$p_{0,x}$	$p_{0,y}$	$p_{1,x}$	$p_{1,y}$	$p_{2,x}$	$p_{2,y}$	$p_{3,x}$	$p_{3,y}$	R	G	B	Opacity	Width
Min.	12	22	-100	-195	-84	-140	-9	22	0	0	0	0	6
Max.	268	273	450	399	465	448	267	305	255	255	255	1	106

Table 7. The value ranges of stroke parameters for each dimension at an image resolution of 295×295 .



Fig. 14. Bézier curves fitted in the same shape as our stroke data.

```

1 from scipy.special import comb
2 def cal_ranking_loss(pred_rank, gt_order, margin=0.125):
3     dif_gt = gt_order - gt_order.t()
4     dif_pred = pred_rank - pred_rank.t()
5     # All pairwise combinations: positions with value 1 indicate that the row corresponds
6     # to a ground truth rendering order earlier than the column.
7     mask = (dif_gt < 0).float()
8     loss_matrix = torch.max(torch.tensor(0.0), (dif_pred - dif_gt * margin) * mask)
9     loss = loss_matrix.sum() / comb(pred_rank.shape[0], 2)
10    return loss
11
12 loss_r = 0.0
13 param, _ = stroke_predictor(canvas1, canvas2)
14 # matching_idx comes from Hungarian matching
15 # -1 takes the ranking dimension
16 pred_rank = param[matching_idx, -1]
17 gt_order = gt_param[valid, -1]
18 loss_r = cal_ranking_loss(pred_rank, gt_order)

```

Listing 1 A simplified code of ranking loss calculation for one stroke sequence.

Stroke parameter fitting (Relevant to Section 3.3 in the Main Text)

In differentiable rasterizer [29], we set the fitting conditions to `[path=1, segment=1]`, ensuring that one cubic Bézier curve corresponds to a single stroke image. Due to the random initialization of the curves, gradient vanishing often occurs during updates when the curve has no overlap with the stroke. To address this, we initially added an optimal transport loss $Loss_{OT}$ for minimizing the distance between distributions, as proposed by [61], to the pixel loss optimization function. However, this approach proved ineffective. In fact, we also tested $Loss_{OT}$ in [61] and observed that when the initial sampling points of a stroke did not overlap with the object in the image (using white-background images), the strokes failed to move toward the object and instead gradually disappeared during backpropagation.

Ultimately, we adopted a more practical solution: detecting the regions with strokes in the image and initializing the curve in those regions. Each stroke's parameters were optimized over 300 iterations to complete the parameterization. Some fitted examples are shown in Figure 14. We present the range of values for each parameter dimension in Table 7, based on images with a resolution of 295×295 pixels.

Code for Ranking Loss (Relevant to Section 3.4 in the Main Text)

Listing 1 presents the core code for calculating the ranking loss of a single set of strokes on a canvas patch. Batch operations are omitted for simplicity.

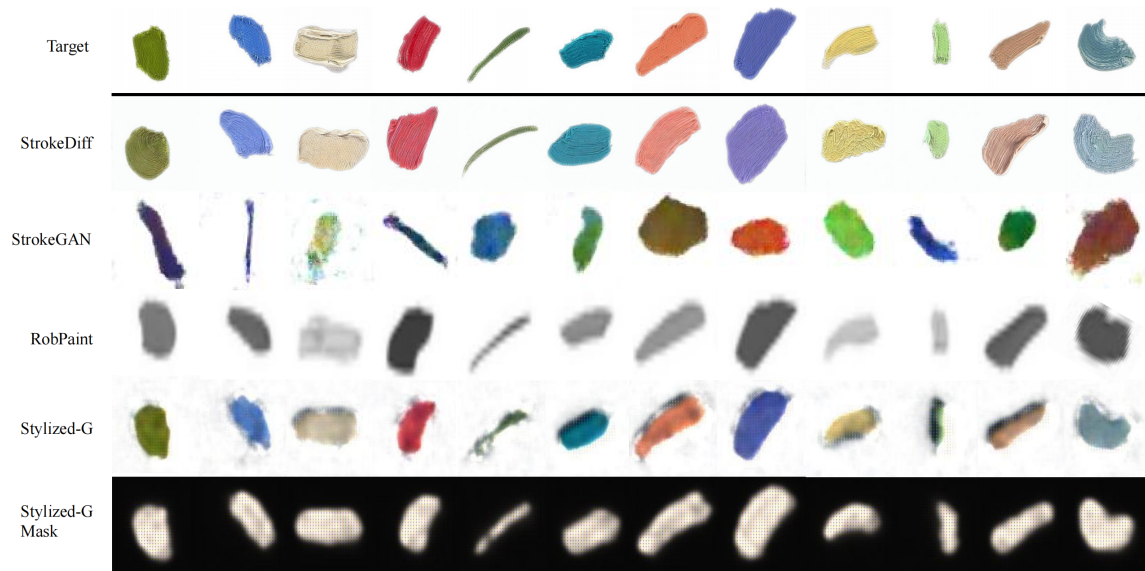


Fig. 15. Comparisons between our stroke generator and StrokeGAN [53], Stylized [61] and RobPaint [1].

Stroke generation comparison (Relevant to Section 4.3.2 in the Main Text)

In Figure 15, we present a qualitative comparison of our results with those generated by other stroke generators. For StrokeGAN, we trained the model for 1000 epochs and selected the best-performing weights from the 700th epoch for comparison. For Stylized-G, we followed the original setup of the method, where stroke parameters excluding RGB were input to the "shading net" to predict the mask, and all parameters were fed into the "rasterization net" to predict the foreground. The model was trained for 370 epochs. For RobPaint, we used the default setting with an output size of $1 \times 16 \times 32$ and trained for 255 epochs.

User study (Relevant to Section 4.4.3 in the Main Text)

Painting quality was evaluated using four questions: Style ("To what extent does the artwork emphasize its oil painting style?"), Aesthetics ("As an artwork, how valuable are they from an aesthetic point of view?"), Texture ("How well are the oil-painting brushstroke textures expressed in the artwork?"), and Content ("From the photograph to the painting, how well is the content applied in the artwork?"). Participants evaluated paintings produced by six methods, with five examples per method.

Received 20 February 2007; revised 12 March 2009; accepted 5 June 2009